

HIGH SPEED FLOW SIMULATION USING OPENFOAM

Luis F. Gutiérrez Marcantoni^{a,b,c}, José P. Tamagno^{a,d} and Sergio A. Elaskar^{a,b,e}

^aDepartamento de Aeronáutica, FCEFyN, Universidad Nacional de Córdoba, Av. Vélez Sarsfield 1601(5000), Córdoba, Argentina

^bConsejo Nacional de Investigaciones Científicas y Técnicas-CONICET

^c*luisgutierrezmarcantoni@conicet.gov.ar*

^d*jose_tamagno@yahoo.com.ar*

^e*selaskar@yahoo.com*

Keywords: openFoam, supersonic flow, *sonicFoam*, PISO, *rhoCentralFoam*, flux interpolation.

Abstract.

It is well known that openFoam has become a very popular tool for research work in different fields and particularly, in fluid dynamics. But, it is also known its lack of detailed documentation supporting solvers made using the set of libraries provided by openFoam. Therefore, it becomes necessary to establish appropriate verifications that can be useful to users going for instance, through the selection of equations discretization schemes from fvSchemes libraries and of solution solvers from fvSolutions libraries, to be later applied in the simulation of a given specific problem. With this purpose, executable solvers available in openFoam 1.7 version to solve supersonic air flow problems are tested. Two different approaches have been taken in developing numerical methods to solve problems in transport phenomena at all Mach numbers and traditionally, they have been referred to as pressure-based and density-based methods. In this work, the advantages or disadvantages in applying any one of these methods, are addressed. To accomplish the proposed tasks, 2D and axisymmetric numerical simulations of well posed problems that have either an analytical solution or available experimental data to compare with, are performed.

1 INTRODUCTION

The finite volume numerical solution of compressible fluid flow equations can be addressed using different approaches i.e, pressure based and density based solvers with the corresponding governing equations solved either in segregated or coupled manners. Within openFoam both approaches are implemented, for instance, the density based *rhoCentralFoam* and the pressure based *sonicFoam*. The main aim of this work is to test the capabilities of these two solvers by the simulation of particular types of compressible fluid flows: the supersonic wedge or ramp, the supersonic diamond airfoil, the two dimensional and the axially symmetric blunt bodies. In the environment that openFoam can display with some solvers, it is possible to select at run time if it will or will not consider the molecular dynamic viscosity and/or turbulence effects on the simulation. Additionally, the numerical scheme for each term in the governing equations can be selected, thus offering the possibility of choosing the best option according to the nature of the problem. openFoam treats coupled equations using a segregated approach, in which equations are formulated for each dependent variable and solved sequentially. Thus, any vector equation is solved by solving each component as a scalar equation, with the possibility of applying iterations over the system of equations until convergence is achieved. Provided that the coupling between the components is not strong, this procedure is quite acceptable ([Weller et al., 1998](#)).

In *sonicFoam*, a non iterative method for handling the coupling of implicitly discretized time dependent fluid flow equations is utilized. The method, known as PISO (for pressure implicit with splitting of operators), is based on the use of pressure and velocity as dependent variables and is applicable to both the incompressible and compressible versions of the transport equations. The main feature of the technique is the splitting of the solution process into a series of steps where operations on pressure are decoupled from those on velocity. With the split, sets of equations being amenable to solution by standard techniques are intended to be produced. The fields obtained after each PISO step, are closer approximations to the exact solution of the difference equations with a formal order of accuracy depending on the number of operation-splitting used. The errors decaying rapidly, together with the fact that the stability of the overall scheme is little impaired by the splitting procedure should allow getting rid of iterations while retaining the advantage of implicit differencing, namely, the ability to cope with large time steps ([Issa, 1985](#)). In this work the PISO methodology is outlined.

The presence of discontinuities, such as shocks and contact surfaces, in high speed compressible flows requires numerical schemes that can capture these features while avoiding spurious oscillations. In notable methods that are effective in producing accurate non oscillatory solutions, the generation of numerical fluxes typically involve Riemann solvers, characteristic decomposition and Jacobian evaluation, making them complex and difficult to implement on a mesh of polyhedral cells that have an arbitrary number of faces. However, an alternative approach exists which does not involve Riemann solvers and can also provide accurate non oscillatory solutions using the so called central schemes. These central schemes implemented in openFoam to be used with *rhoCentralFoam*, were proposed by ([Kurganov and Tadmor, 2000](#); [Kurganov et al., 2000](#)) and ([Greenshields et al., 2010](#)). It shall be pointed out that Romanelli et al. (2010) , have successfully developed within the openFoam framework, a solver that involve the use of Riemann solvers, but it is not included in the libraries currently provided by openCFD®.

2 GOVERNING EQUATIONS

It is intended to solve the standard governing fluid equations in an Eulerian frame of reference:

- Mass conservation

$$\frac{\partial \rho}{\partial t} + \nabla \cdot (\rho \mathbf{U}) = 0 \quad (1)$$

- Conservation of momentum (neglecting body forces)

$$\frac{\partial(\rho \mathbf{U})}{\partial t} + \nabla \cdot (\rho \mathbf{U} \mathbf{U}) = \nabla p + \nabla \cdot \underline{\tau} \quad (2)$$

where ρ is the mass density, \mathbf{U} the fluid velocity, p the pressure and $\underline{\tau}$ is the viscous stress tensor. Following the assumption proposed by Boussinesq the stress tensor can be represented by:

$$\underline{\tau} = 2\mu \text{dev}(\underline{\mathbf{D}}) \quad (3)$$

In Eq.(3), μ is the dynamic viscosity, $\underline{\mathbf{D}} = \frac{1}{2}[\nabla \mathbf{U} + (\nabla \mathbf{U})^T]$ is the deformation gradient tensor and $\text{dev}(\underline{\mathbf{D}}) = \underline{\mathbf{D}} - \frac{1}{3} \text{tr}(\underline{\mathbf{D}}) \mathbf{I}$ is its deviator component. \mathbf{I} is the unit tensor.

- Conservation of energy

The corresponding balance equations are written in terms of the total non chemical energy (E) and the sensible energy (e_s). These energies are defined by:

$$e_s = h_s - \frac{p}{\rho} = \int_{T_0}^T C_v dT - RT_0/W \quad (4)$$

$$E = H - \frac{p}{\rho} = e_s + \frac{1}{2} \mathbf{U} \cdot \mathbf{U} \quad (5)$$

being h_s the sensible enthalpy ($h_s = \int_{T_0}^T C_p dT$) and H the total enthalpy ($H = h_s + \frac{1}{2} \mathbf{U} \cdot \mathbf{U}$). Then the energy balance equations can be written:

$$\frac{\partial(\rho e_s)}{\partial t} + \nabla \cdot [\mathbf{U}(\rho e_s)] + \nabla \cdot \mathbf{q} + (p \mathbf{I} - \underline{\tau}) \nabla \cdot \mathbf{U} = 0 \quad (6)$$

$$\frac{\partial(\rho E)}{\partial t} + \nabla \cdot [\mathbf{U}(\rho E)] + \nabla \cdot \mathbf{q} + \nabla \cdot [(p \mathbf{I} - \underline{\tau}) \mathbf{U}] = 0 \quad (7)$$

It is assumed that the working gas (air), behaves like one component (frozen mixture composition) perfect caloric gas. In this context the following relations are applicable

$$e_s = \left(C_p - \frac{R_u}{W} \right) T = C_v T \quad (8)$$

$$T = \frac{1}{C_v} \left[\frac{(\rho E)}{\rho} - \frac{1}{2} \mathbf{U} \cdot \mathbf{U} \right] \quad (9)$$

$$p = \rho \frac{R_u}{W} T = \frac{\rho}{\psi} \quad (10)$$

where ψ is the air compressibility, R_u is the universal gas constant and $\gamma = \frac{C_p}{C_v}$ is the ratio of specific heats at constant pressure and volume, C_p and C_v respectively. Additionally, the heat flux (\mathbf{q}) can be represented solely by Fourier's law ($\mathbf{q} = -\lambda T$) where T is the temperature and λ the conductivity. If $\underline{\tau} = 0$ and $\mathbf{q} = 0$, the flow is inviscid and the conservation equations reduce to Euler's equations.

Mean quantities conservation equations to be used in compressible flow RANS simulations, are written in terms of Favre's mass weighted averages (Favre, 1969; Wilcox, 1998). Any dependent variable f can be split into mean and fluctuating components by writing $f = \tilde{f} + f''$. However, in Favre's particular way of averaging the product $\rho f'' = 0$ (rather than $f'' = 0$ itself) and consequently, the mean value becomes

$$\tilde{f} = \frac{\overline{\rho f}}{\bar{\rho}} \quad (11)$$

Using Favre's way of making averages the instantaneous conservation equations can be written as follows

- Mass

$$\frac{\partial \bar{\rho}}{\partial t} + \nabla \cdot (\bar{\rho} \tilde{\mathbf{U}}) = 0 \quad (12)$$

- Momentum

$$\frac{\partial(\bar{\rho} \tilde{\mathbf{U}})}{\partial t} + \nabla \cdot [\tilde{\mathbf{U}}(\bar{\rho} \tilde{\mathbf{U}})] + \nabla \bar{p} - \nabla \cdot (\underline{\tau} + \underline{\tau}_t) = 0 \quad (13)$$

where $\underline{\tau}_t = 2\mu_t \text{dev}(\tilde{\mathbf{D}})$. It is now possible, to introduce an effective $\mu_{eff} = \mu + \mu_t$ if the molecular viscous stress tensor is constructed using the mean deformation gradient tensor $\tilde{\mathbf{D}}$, and the turbulent dynamic viscosity μ_t needed to build the turbulent Reynolds stresses, has been evaluated. This evaluation can be accomplished defining a turbulence model.

- Energy

$$\frac{\partial(\bar{\rho} \tilde{e}_s)}{\partial t} + \nabla \cdot [\tilde{\mathbf{U}}(\bar{\rho} \tilde{e}_s)] - \nabla \cdot (\alpha_{eff} \nabla \tilde{h}_s) + \bar{p} \nabla \cdot \tilde{\mathbf{U}} = 0 \quad (14)$$

The effective thermal diffusivity ($\alpha_{eff} = \alpha + \alpha_t$) include both, the local mean molecular and the turbulent. The sensible enthalpy is calculated as $\tilde{h}_s = \tilde{e}_s + \frac{\bar{p}}{\bar{\rho}}$.

$$\frac{\partial(\bar{\rho} \tilde{E})}{\partial t} + \nabla \cdot [\tilde{\mathbf{U}}(\bar{\rho} \tilde{E})] - \nabla \cdot (\alpha_{eff} \nabla \tilde{h}_s) + \nabla \cdot (\bar{p} \tilde{\mathbf{U}}) = 0 \quad (15)$$

from the definition of total energy the sensible enthalpy can be calculated as $\tilde{h}_s = \tilde{E} + \frac{\bar{p}}{\bar{\rho}} - \frac{1}{2} \tilde{\mathbf{U}} \cdot \tilde{\mathbf{U}}$. Notice that in both energy equations the term associated with the molecular viscous heating has been neglected.

3 COMPUTATIONAL METHODS

The two main differences between *sonicFoam* and *rhoCentralFoam* are: the use of pressure and velocity as dependent variables through the PISO method in *sonicFoam*, and the use of an alternative approach to Riemann solvers based on central-upwind schemes in *rhoCentralFoam*. Both computational solvers schemes will briefly be described next.

3.1 The sonicFoam

The required pressure equation to be used in *sonicFoam*, may be derived from the differential form of the momentum and continuity equations. This practice, however has its disadvantages, since it is not easy to ensure that all terms in the pressure equation are discretized in a manner consistent with the discretisation of the corresponding terms in the parent equations. As a consequence of this inconsistency, the pressure thus obtained may not always yield a velocity field which satisfy both the momentum and continuity equations simultaneously. Since satisfaction of the continuity equation is a basic requisite of the solution of the pressure equation, the above mentioned incompatibility is unacceptable. Alternatively the pressure equation may be derived from the discrete forms of the momentum and continuity equations (Issa, 1985). It is this practice which has here been adopted.

The transport equations stated above are now expressed in finite difference form. There are numerous ways of representing the spatial and temporal derivatives in the parent equations (momentum and continuity), however the discretized equations are here formulated using the Euler implicit difference scheme Then, for compressible flows the governing equations Eq.(1), Eq.(2) and Eq.(7) may be expressed in difference form for each mesh point as

$$\frac{1}{\Delta t}(\rho^{n+1} - \rho^n) + (\rho u_i)_{,i}^{n+1} = 0 \quad (16)$$

$$\frac{1}{\Delta t} [(\rho u_j)^{n+1} - (\rho u_j)^n] = -S_{ij,i}^{n+1} - (p)_{,j}^{n+1} \quad (17)$$

$$\frac{1}{\Delta t} [(\rho E)^{n+1} - (\rho E)^n] + (\rho Eu_i)_{,i}^{n+1} = -(pu_i)_{,i}^{n+1} - (\tau_{ij}u_i)_{,j}^{n+1} \quad (18)$$

where n and $n + 1$ denote successive time levels. $S_{ij,i}$ stands for the finite difference representation of the convective and diffusive fluxes of momentum. The operator $()_{,i}$ is the finite difference equivalent to $\frac{\partial}{\partial x_i}$. In order to increase stability and accuracy, $S_{ij,i}$ is split into diagonal (D) and non diagonal (N) terms (Chung, 2010).

$$S_{ij,i} = S_{ij,i}^{(D)} + S_{ij,i}^{(N)} = A_{ji}^{(D)}u_i + S_{ij,i}^D \quad (19)$$

In the PISO scheme, the conservation of mass has to be satisfied within predictor-corrector steps. The predictor-corrector steps are, after (Chung, 2010), as follows

3.1.1 Two-stage scheme

Momentum predictor

The equation for momentum (Eq.(17)) is solved in this step implicitly, using old time pressures and density, as

$$\left(\frac{\delta_{ij}}{\Delta t} + \frac{A_{ji}^{(D)}}{\rho^n} \right) (\rho^n u_i^*) = -S_{ij,i}^{(N)} - p^n_{,j} + \frac{\rho^n u_i^n}{\Delta t} \quad (20)$$

The solution of this equation yields u_i^* .

Momentum corrector step

The momentum equation is now written in the explicit corrector form

$$\left(\frac{\delta_{ij}}{\Delta t} + \frac{A_{ji}^{(D)}}{\rho^n} \right) (\rho^* u_i^{**}) = -S_{ij,i}^{*(N)} - p^*,_j + \frac{\rho^n u_i^n}{\Delta t} \quad (21)$$

which by subtracting Eq.(20) from it, can be rewritten in incremental form as

$$\rho^* u_i^{**} - \rho^n u_i^* = - \left(\frac{\delta_{ij}}{\Delta t} + \frac{A_{ji}^{(D)}}{\rho^n} \right)^{-1} (p^* - p^n),_j \quad (22)$$

The continuity equation is now taken in the form

$$(\rho^* u_i^{**}),_i = -\frac{1}{\Delta t} (\rho^* - \rho^n) \quad (23)$$

Differentiating Eq.(22) and using Eq.(23) it is obtained

$$\left[\left(\frac{\delta_{ij}}{\Delta t} + \frac{A_{ji}^{(D)}}{\rho^n} \right)^{-1} (p^* - p^n),_j \right]_{,i} = (\rho^n u_i^*),_i + \frac{1}{\Delta t} (\rho^* - \rho^n) \quad (24)$$

Using the equation of state (Eq.(10)) in the form $\rho = p \psi^n$ the Eq.(24) becomes

$$\left[\left(\frac{\delta_{ij}}{\Delta t} + \frac{A_{ji}^{(D)}}{\rho^n} \right)^{-1} (p^* - p^n),_j \right]_{,i} - \frac{\psi^n}{\Delta t} (p^* - p^n) = (\rho^n u_i^*),_i \quad (25)$$

This is the pressure equation which, when solved yields the p^* field. The equation of state can then be used to determine the density ρ^* , and the Eq.(22) to compute u_i^{**} .

The energy predictor step

The energy equation (Eq.(18)) may now be solved in the implicit form

$$\left(\frac{1}{\Delta t} + \frac{B^{(D)}}{\rho^*} \right) (\rho^* E^*) = -(\rho E u_i)^{*N},_i - (\rho^* u_i^{**}),_i + (\tau_{ij} u_i^{**})_i + \frac{\rho^n E^n}{\Delta t} \quad (26)$$

with $B^{(D)}$ being the diagonal component of the convective term. The value T^* can now be evaluated from E^* and u_i^{**} .

Second momentum corrector step

For this step the momentum equation is

$$\left(\frac{\delta_{ij}}{\Delta t} + \frac{A_{ji}^{(D)}}{\rho^*} \right) (\rho^{**} u_i^{***}) = -S_{ij,i}^{**N} - p^{**},_j + \frac{\rho^n u_i^n}{\Delta t} \quad (27)$$

which in incremental form becomes

$$\begin{aligned} \rho^{**} u_i^{***} - \rho^* u_i^{**} = & \\ & \left(\frac{\delta_{ij}}{\Delta t} + \frac{A_{ji}^{(D)}}{\rho^*} \right)^{-1} \left[-S_{ij,i}^{**N} + S_{ij,i}^{*(N)} - A_{ij} \frac{\rho^* - \rho^n}{\rho^n} u_i^{**} - (p^{**} - p^*),_j \right] \end{aligned} \quad (28)$$

By combining with the continuity relation

$$(\rho^{**} u_i^{**})_{,i} = -\frac{1}{\Delta t} (\rho^{**} - \rho^*) \quad (29)$$

the following pressure equation is obtained

$$\begin{aligned} & \left[\left(\frac{\delta_{ij}}{\Delta t} + \frac{A_{ji}^{(D)}}{\rho^*} \right)^{-1} (p^{**} - p^*)_{,j} \right]_{,i} - \frac{\psi^*}{\Delta t} (p^{**} - p^*) = \\ & \left[\left(\frac{\delta_{ij}}{\Delta t} + \frac{A_{ji}^{(D)}}{\rho^*} \right)^{-1} \left\{ \left(-S_{ki,k}^{*(N)} \right. \right. \right. \\ & \left. \left. \left. + S_{ki,k}^{*(N)} \right) - A_{ji} \left(\frac{\rho^* - \rho^n}{\rho^n} \right) u_i^{**} \right\} \right]_{,i} + \\ & \frac{p^*}{\Delta t} (\psi^* - \psi^n) \end{aligned} \quad (30)$$

Notice that in arriving at the last equation the following equation of state has been invoked

$$\rho^{**} = p^{**} \psi^* \quad (31)$$

Solution of Eq.(30) yields p^{**} , while Eq.(31) and Eq.(28) are used to evaluate ρ^{**} and u^{***} , respectively, which together with T^* are used to represent the field values at the new time level $n + 1$. The formal order of accuracy of the two-stage scheme developed is second order (in discretisation errors) (Issa, 1985). To achieve a higher formal order an additional correction stage has to be introduced to the steps presented above. This implies that the T^* , u_i^{***} , p^{**} and ρ^{**} fields have to be again updated. The procedure to be followed is given by (Issa, 1985; Chung, 2010)

3.2 The rhoCentralFoam

In compressible fluid flows, properties are not only transported by the flow, but also by the propagation of waves. This requires the construction of flux interpolations that take into account that transports can occur in any direction. Since the interpolations are from neighboring cell values to a given face only, the (Kurganov and Tadmor, 2000), and (Kurganov et al., 2000) methods can be applied.

The convective terms of the conservation equations listed in section 2 and applicable to *rhoCentralFoam*, are of the form $\nabla \cdot [\mathbf{U}\rho]$, $\nabla \cdot [\mathbf{U}(\rho\mathbf{U})]$, $\nabla \cdot [\mathbf{U}(\rho E)]$ and $\nabla \cdot [\mathbf{U}p]$. Each is integrated over a control volume and linearized as follows

$$\int_V \nabla \cdot [\mathbf{U}\Psi] dV = \sum_f [\mathbf{S}_f \cdot \mathbf{U}_f] \Psi_f \approx \sum_f \phi_f \Psi_f \quad (32)$$

where \sum_f denotes summation over all faces and $\phi_f = \mathbf{S}_f \cdot \mathbf{U}_f$ is the volumetric flux, i.e. the volume of fluid flowing through the face per second. To obtain Ψ_f by splitting the flux in two directions, namely outgoing and incoming to the face “owner” cell, the following scheme is used

$$\sum_f \phi_f \Psi_f = \sum_f [\alpha \phi_{f+} \Psi_{f+} + (1 - \alpha) \phi_{f-} \Psi_{f-} + \omega_f (\Psi_{f-} - \Psi_{f+})] \quad (33)$$

where f_+ and f_- denote directions coinciding with the directions $+S_f$ and $-S_f$, respectively. The first two terms on the right hand side of Eq.(33) are flux evaluations in the f_+ and f_- directions. The third term is required in cases where the convection term is part of a substantial derivative, e. g. $\frac{\partial(\rho u_i)}{\partial t} + \nabla \cdot [U(\rho u_i)]$. It is an additional diffusion term using a volumetric flux ω_f based on the maximum speed of propagation of any discontinuity that may exist at a face between values interpolated in the f_+ and f_- directions (Greenshields et al., 2010).

Volumetric fluxes associated with the local speed of propagation can be calculated as follows:

$$\varphi_{f+} = \max(a_{f+} | S_f | + \phi_{f+}, a_{f-} | S_f | + \phi_{f-}, 0) \quad (34)$$

$$\varphi_{f-} = \max(a_{f+} | S_f | - \phi_{f+}, a_{f-} | S_f | - \phi_{f-}, 0) \quad (35)$$

where, $a_{f\pm} = \sqrt{\gamma \frac{R_u}{W} T_{f\pm}}$ are the speeds of sound of the gas at the face, outgoing and incoming to the owner cell. If in Eq.(33) the weighted coefficient of f_+ and f_- contributions is $\alpha = 0.5$, the scheme is termed central. Schemes on which the weighting is biased in the upwind direction by means of the factor $\alpha = \frac{\varphi_{f+}}{(\varphi_{f+} - \varphi_{f-})}$, are termed central upwind. The diffusive volumetric flux term ω_f is determined according to (Greenshields et al., 2010), as

$$\omega_f = \begin{cases} \alpha \max(\varphi_{f+}, \varphi_{f-}) & \text{for Kurganov and Tadmor scheme} \\ \alpha(1-\alpha)(\varphi_{f+} + \varphi_{f-}) & \text{for Kurganov, Noelle and Petrova scheme} \end{cases} \quad (36)$$

To switch between low and high order schemes, the interpolation procedure uses a flux limiter function $\beta(r)$, where r represents the ratio of successive gradients of the interpolated variable (constrained to $r \geq 0$). The van Leer, Minmod and van Albada limiter functions given by

VanLeer	$\frac{r+ r }{1+r}$
VanAlbada	$\frac{r+r^2}{1+r^2}$
Minmod	$\max(0, \min(1, r))$

Table 1: VanLeer, VanAlbada and Minmod limiter functions

were selected for the f_+ and f_- interpolations of all flow variables. For example, the f_+ interpolation of Ψ is simply evaluated according to

$$\Psi_{f+} = (1 - g_{f+})\Psi_P + g_{f+}\Psi_N \quad (37)$$

where $g_{f+} = \beta(1 - w_f)$. Subscripts P and N indicate the face owner cell and the neighboring cell, respectively. The weighting coefficient $w_f = |S_f \cdot d_{fN}| / |S_f \cdot d_{PN}|$, expresses that the vector d connects the centroid of the owner cell P to that of neighboring cell N and the vector d_{fN} connects the centre of the face to the centroid of the cell N (Fig.(1)).

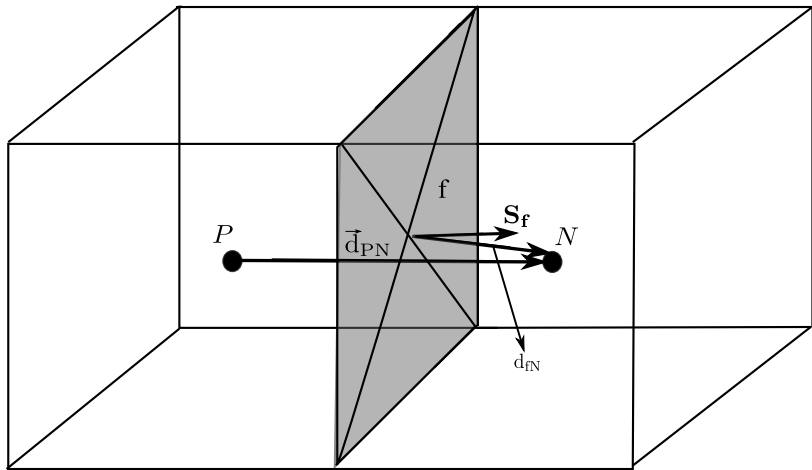


Figure 1: Finite volume discretization

Gradient terms present in the fluid governing equations are integrated over a control volume and discretized as follows

$$\int_V \nabla \Psi dV = \int_S d\mathbf{S} \Psi \approx \sum_f \mathbf{S}_f \Psi_f \quad (38)$$

In gradients terms, the Kurganov and Tadmor, and Kurganov, Noelle and Petrova schemes split the interpolation procedure into f_+ and f_- directions according to

$$\sum_f \mathbf{S}_f \Psi_f = \sum_f [\alpha \mathbf{S}_f \Psi_{f+} + (1 - \alpha) \mathbf{S}_f \Psi_{f-}] \quad (39)$$

The f_+ and f_- interpolation uses the limiter previously described. In this work, the rhoCentralFoam is tested as a solver for inviscid supersonic flow problems. Therefore, the discretization of Laplacian terms with diffusion coefficient is not presented.

4 TEST CASES

Here are presented four test cases to study the performances of the selected solvers *sonicFoam* and *rhoCentralFoam*, with simulations in supersonic flow. The first case is a supersonic flow over a wedge, the second one the flow over a supersonic diamond airfoil and the last two are flows over a two dimensional and axially symmetric blunt bodies. In all cases comparisons with available analytical or numerical solutions will be presented.

4.1 Wedge

As first glance to the behavior of the solvers *sonicFoam* and *rhoCentralFoam* in handling supersonic flow problems, the simple wedge (Fig.(2)) is considered. The free stream or inlet conditions are denoted by subscript ∞ and the conditions downstream the wave by subscript 2. Solvers quality are in this case determined by the accuracy with which the shock angle (θ_s) and downstream flow conditions for a given wedge angle (θ_w), are predicted. The wedge angle is chosen 15° and the case is solved for a set of Mach numbers $M_\infty = [1.65, 1.75, 2, 2.25, 2.5, 3, 3.5]$. The analytical solution of this problem is well known and it can be found in a wide range of bibliography (Anderson, 2004)

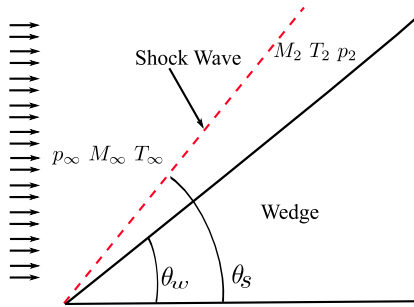


Figure 2: Wedge configuration

A mesh with 50000 hexahedral cells is used in the simulation. For the downstream flow region or outlet it is imposed the *waveTransmissive* boundary property. This boundary property is considered appropriate since account for all incoming waves and does not permit any reflection. (for more details see (Poinsot and Lele, 1992)). The free stream pressure and temperature are taken as $T_\infty = 270$ K and $p_\infty = 100$ Kpa.

As it was early mentioned all computation for this case will be compared with values obtained from the oblique shock theory, they are: downstream average Mach number, wave angle, pressure and temperature ratios as function of all free stream Mach numbers listed above. From Fig.(3) it can be observed that in a global sense all quantities of interest obtained with *rhoCentralFoam* show equal or better accuracy than those calculated by *sonicFoam*. However temperature values computed with *sonicFoam* are in poor agreement when compared with analytical predictions, and as the Mach number increases the disagreement becomes greater. On the other hand, the numerical simulation with *rhoCentralFoam* offers good approximation and apparently, regardless of M_∞ .

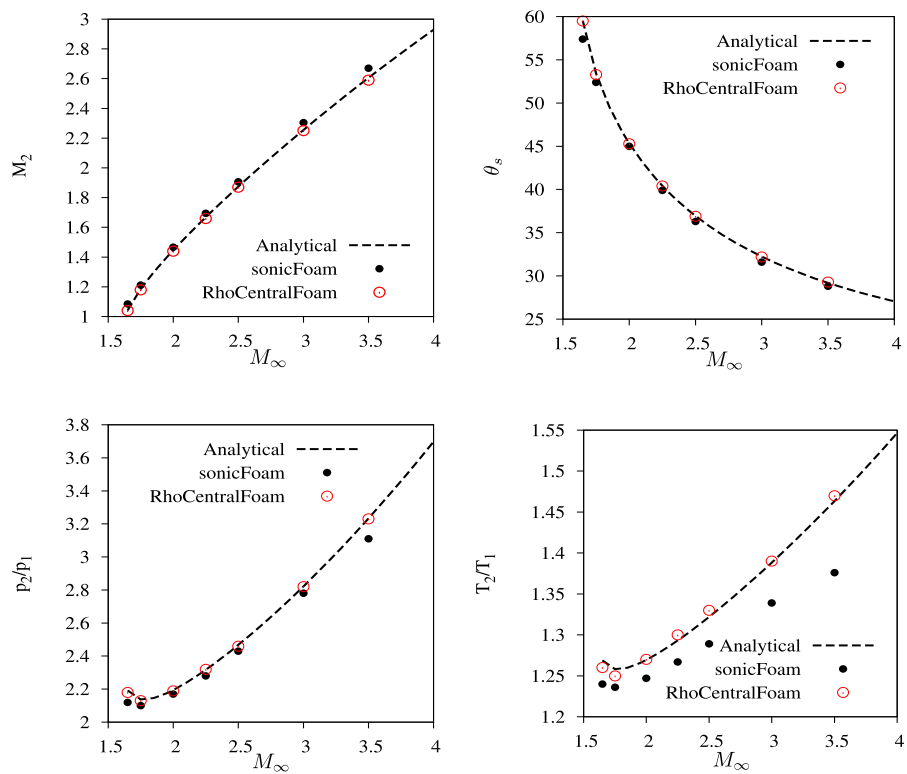


Figure 3: Downstream Mach number, wave angle, pressure and temperature ratios

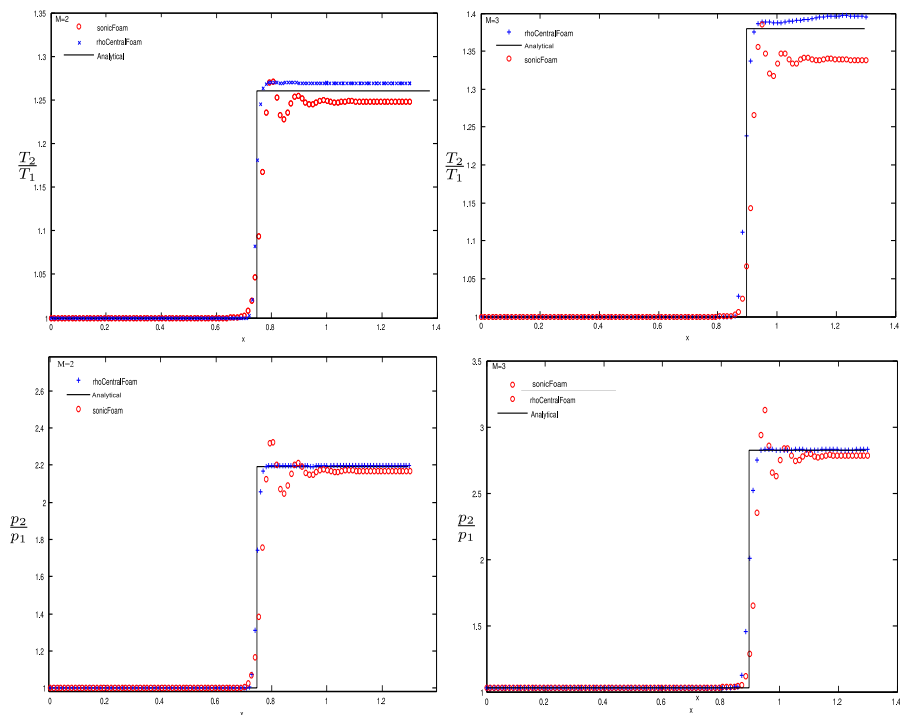


Figure 4: Positioning, pressure and temperature ratios

Fig.(4) shows pressure and temperature ratios across the shock, obtained with *rhoCentralFoam* and *sonicFoam* and are compared with analytical solutions. Both solvers give good results for the shock position, but again *rhoCentralFoam* provides the best approximation. Notice the computed temperature differences and the oscillations induced by *sonicFoam*. These oscillations are practically absent in the *rhoCentralFoam* calculations.

4.2 Diamond Airfoil

The test case simulate a supersonic flow over a diamond type airfoil shown in Fig.(5).

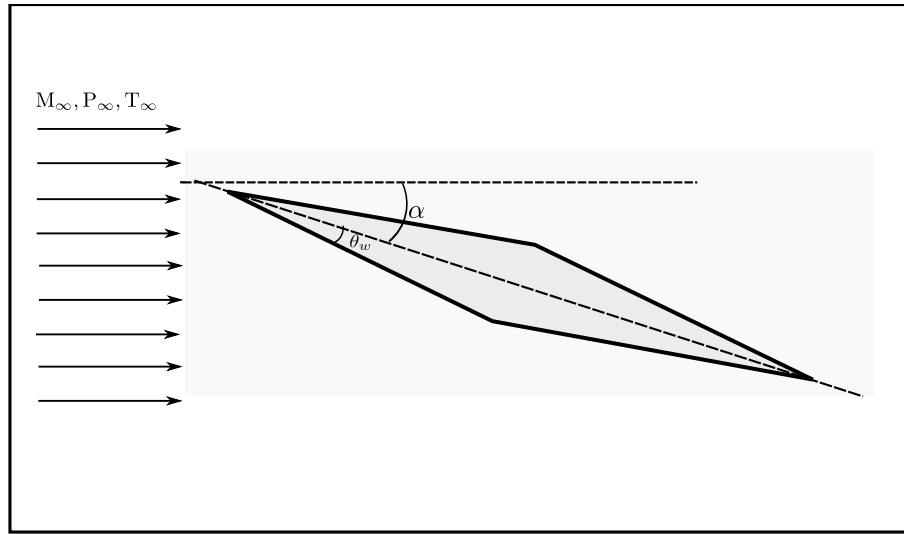


Figure 5: Diamond airfoil configuration

Here θ_w is the wedge angle of the airfoil, α the angle of attack, and the free stream flow properties are those with ∞ subscript. By making a qualitative analysis of the flow around the body for $\alpha > 0$, as Fig.(6) shows, it is expected:

- between regions I and II; expansion fan
- between regions II and III; expansion fan
- between regions I and IV; shock wave
- between regions IV and V; expansion fan
- between regions III and VI; shock wave

The exception is between regions V and VI, where the type of flow can be set only by calculations. Therefore going from regions I to II, II to III and IV to V, it will be seen a velocity increase, and decreasing density, pressure and temperature. The opposite will be for regions I to IV and III to VI. All these changes in flow velocity and flow states, can be calculated using Prandtl-Meyer expansion and oblique shock theories. In region VI should appear a slip line through which there are differences in velocity, but not in pressure. This is due to the fact that in arriving to region VI by the upper side, not necessarily the same values are obtained when the arriving by the lower side.

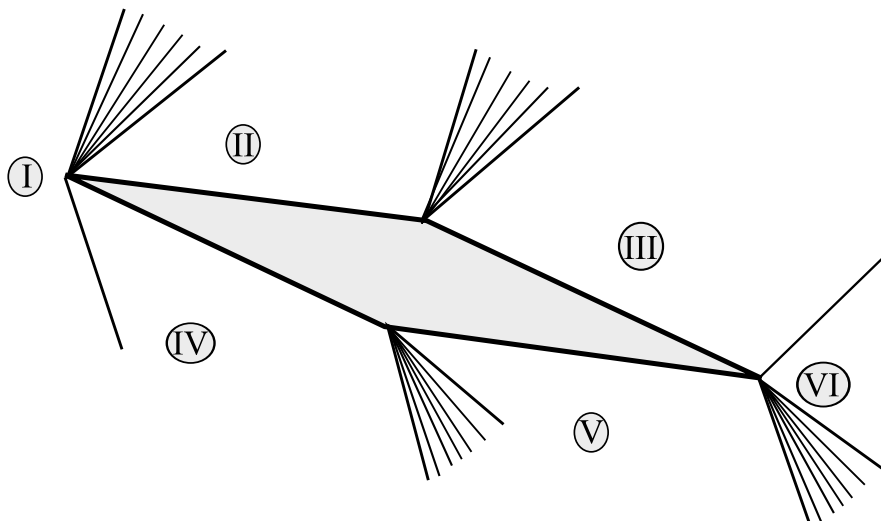


Figure 6: Flow field regions

The analysis of this problem is restricted to an angle of attack of 15° and a wedge angle of 10° . To run the case with *sonicFoam* a mesh with 285300 cells is required, while *rhoCentralFoam* does the same run and obtain the same results, utilizing a mesh of 86300 cells. In Table.(2) are presented the Mach number and pressure relations for each region defined in Fig.(6).

Region	Analytical Solution		<i>sonicFoam</i>		<i>rhoCentral</i>	
	M	P_r/P_1 ¹	M	P_r/P_1	M	Pressure
II	3.27	0.67	3.28	0.65	3.27	0.66
III	4.78	0.09	4.78	0.086	4.8	0.087
IV	1.73	4.88	1.88	4.85	1.71	4.86
V	2.48	1.51	2.47	1.33	2.46	1.56

Table 2: Diamond airfoil pressure ratio and Mach number

From Table.(2) it is observed that in a global sense the predictions of both solvers are of good quality, but from the computational cost point of view, it must be taken into account that the mesh needed to obtain good results with *sonicFoam* has around 3.3 times more cells than used with *rhoCentralFoam*. In addition it can be seen that the pressure computed in region V by *sonicFoam* shows the highest percent of error (12%).

¹Subscript r makes reference to regions I,II,...V

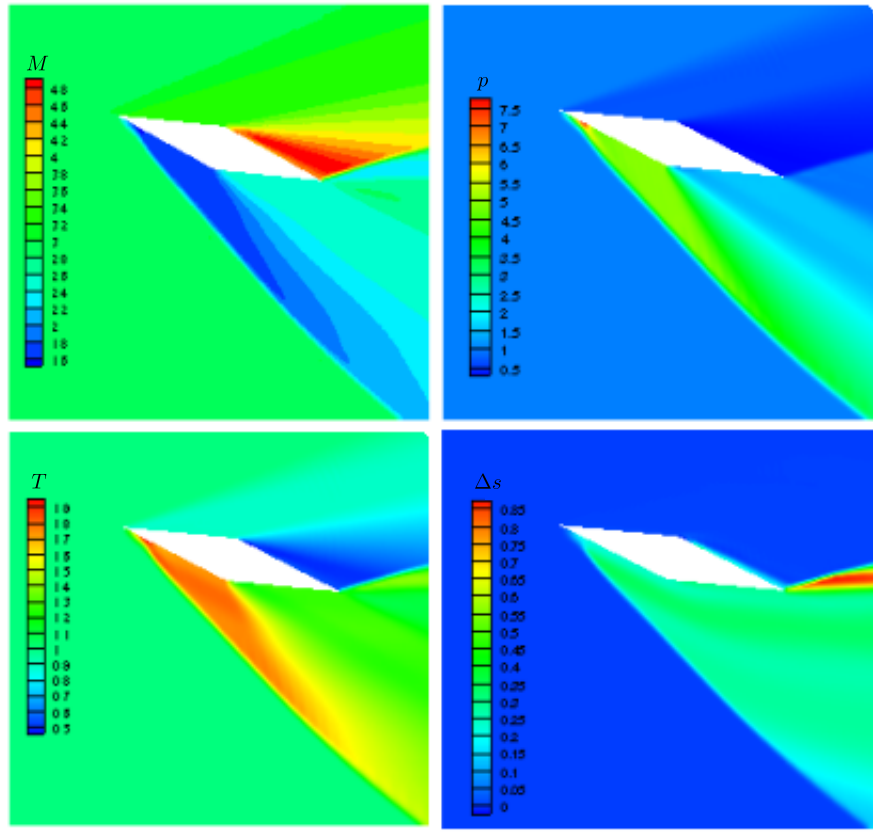


Figure 7: Flow field variables predictions with *rhoCentralFoam*

In Fig.(7) are shown Mach number, pressure, temperature, and entropy fields predicted with *rhoCentralFoam*, which are in agreement with the above written expectations. In the Mach number field are clearly seen shock waves and expansion fans. Also from Mach, pressure and temperature fields it can be observed that between region V to VI there is an expansion fan and between regions III and IV there is a shock. Finally from the entropy field it can be conclude that the computation does not violate the entropy behavior through discontinuities and continuous waves. Notice that in region VI the slip line is visible, and the entropy field confirm that its behavior is consistent with the theory in the sense that entropy shows a discontinuity but the pressure is constant.

4.3 Flow over a two dimensional blunt body

The next analysis related to performances of selected openFoam solvers, applies to the supersonic flow around a 2D blunt body. The contour of this blunt body is described by the relation:

$$f(x) = x^{-0.5} \quad \text{for } 0 \leq x \leq 1 \quad (40)$$

The problem is solved using two meshes, being each one constructed using a single block of hexahedral cells. One mesh has 45000 cells and the other 72000 cells, the mesh configuration can be seen in Fig.(8). The free stream conditions are the same that in (Brooks and Powers, 2004), $M_\infty = 3.5$, $T_\infty = 1$ and $p_\infty = 1$ (values corresponding to a normalized air).

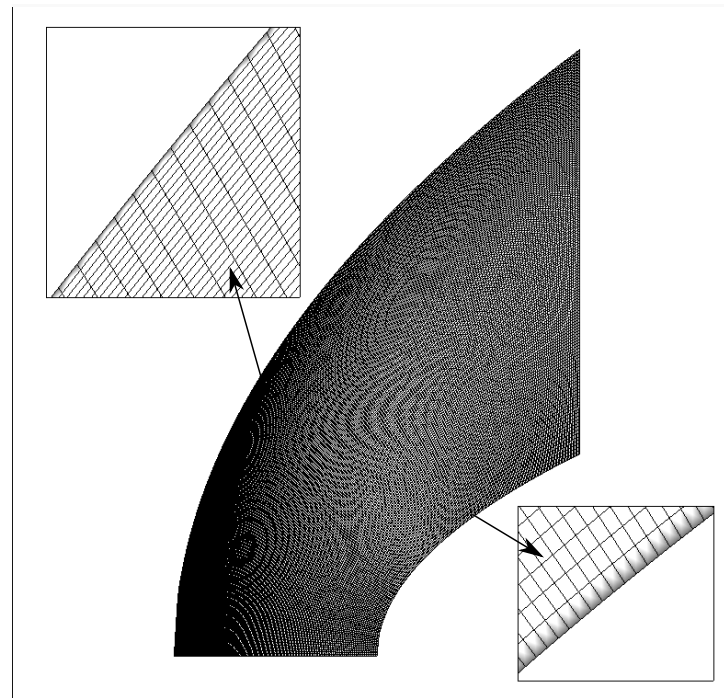


Figure 8: Two dimensional blunt body mesh configuration

The blunt body problem is solved over the above described meshes by using the Minmod, van Leer and van Albada limiter functions. In Fig.(9) and Fig.(10) are shown contour plots for Mach number and pressure fields obtained using each one of the limiters. From these figures it can be seen that the Minmod limiter gives a more diffusive description of the shock, the van Leer and van Albada limiter functions reduce shock diffusivity, but have shown a tendency to induce oscillations in the pressure field calculations. The van Albada limiter gives the better definition of the shock wave, but oscillations in the pressure field are stronger. The described behavior, provide an indication that the best balance between free oscillations pressure calculations and shock wave definition is obtained by using the van Leer limiter function. The impact pressure ratio predicted from the classical normal shock theory is $\frac{P_o}{P_\infty} = 16.24$ ([Anderson, 2004](#)). Numerical predictions for each of the considered limiter functions are shown in Table.(3).

$\beta(r)$	Impact Pressure	%Error
VanLeer	16.21	0.18
Minmod	16.34	0.6
VanAlbada	16.22	0.12

Table 3: Impact pressure error (Mesh1)

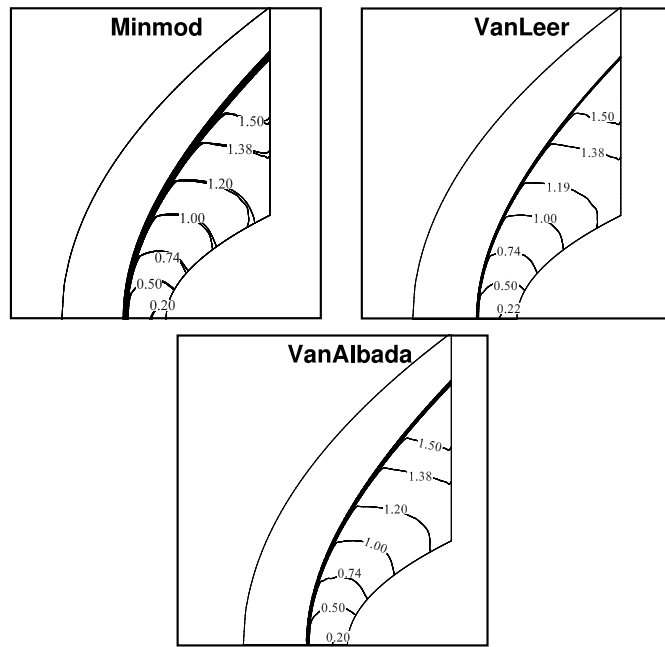


Figure 9: Mach contour lines (Mesh1)

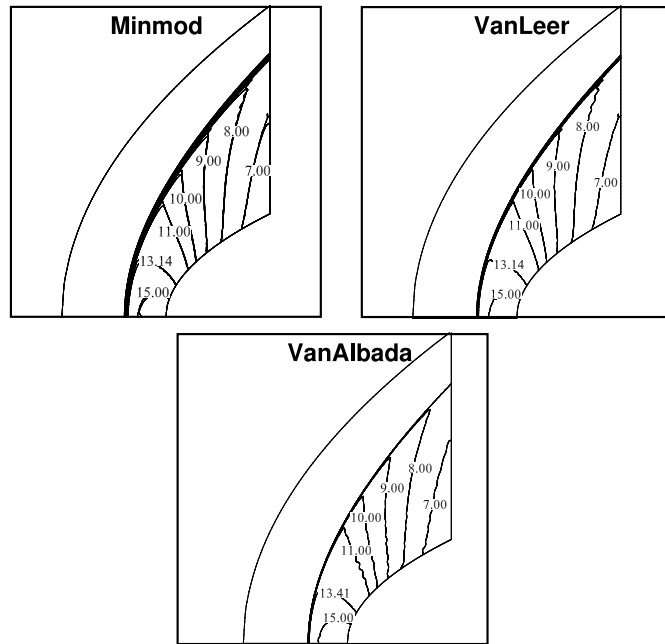


Figure 10: Pressure contour lines (Mesh1)

In Fig.(11) calculation of entropy fields corresponding to each of the limiters listed in Table.(1), are shown. From this figure it is clear that the computations satisfies the entropy changes across the curved shock wave, hence the solution can be considered correct.

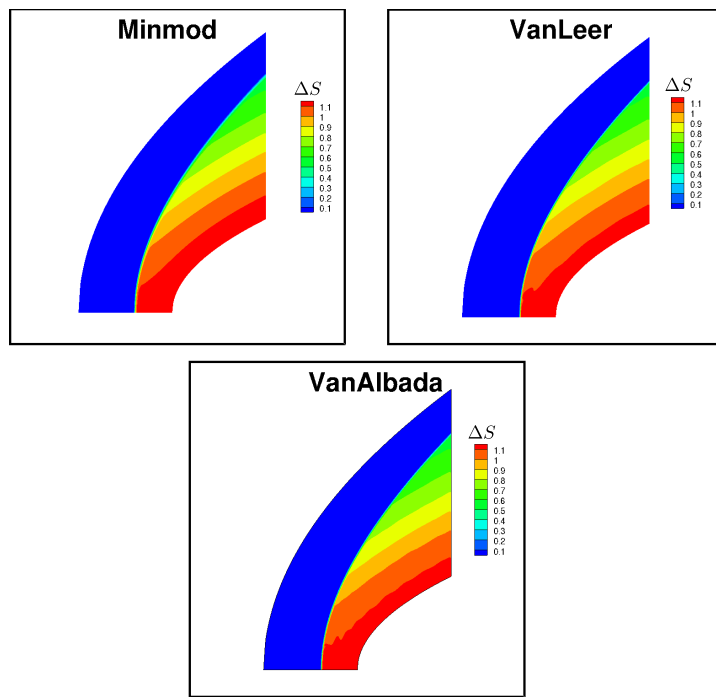


Figure 11: Entropy fields (Mesh1)

The pressure and Mach contour plots for the mesh with the larger number of cells can be seen in Fig.(12) and Fig.(13). From these figures it can be observed that the mesh refinement tends to reduce diffusivity shown in previous fields prediction by using the Minmod limiter, and oscillations practically disappear in pressure calculations using van Albada and van Leer limiters, finally with respect at shock wave capturing, appears that the van Albada limiter gives the better resolution ².

²The ability of the simulation procedure to compute shock-body distance has been verified running cases on which Billig's correlations is applicable (Billig, 1967). Greater found discrepancies are of the order of 6%

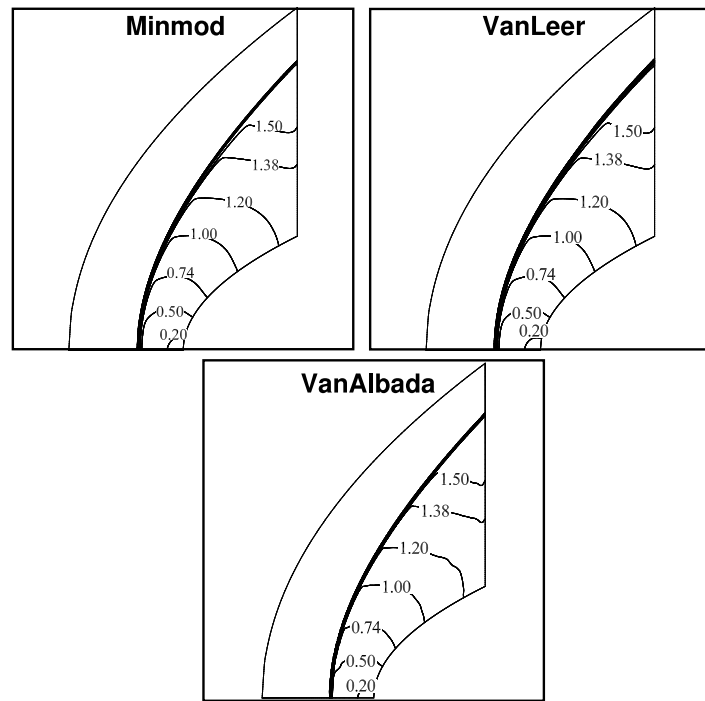


Figure 12: Mach contour lines (Mesh2)

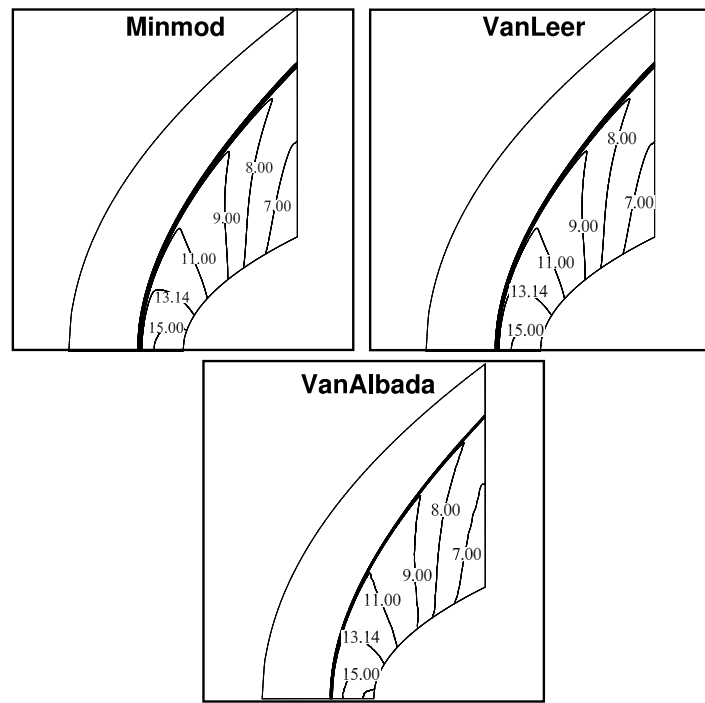


Figure 13: Pressure contour lines (Mesh2)

4.4 Flow over an axially symmetric blunt body

Here is presented the numerical simulation of the flow around an axially symmetric blunt body whose generatrix is the contour (Eq.(40)) of the previous two dimensional blunt body. The results of this simulation being more amenable to compare with Newtonian theory results

(Anderson, 2006). The inlet flow conditions are the same used in the two dimensional blunt body: $M_\infty = 3.5$, $T_\infty = 1$ and $p_\infty = 1$ (after selection of a normalized gas).

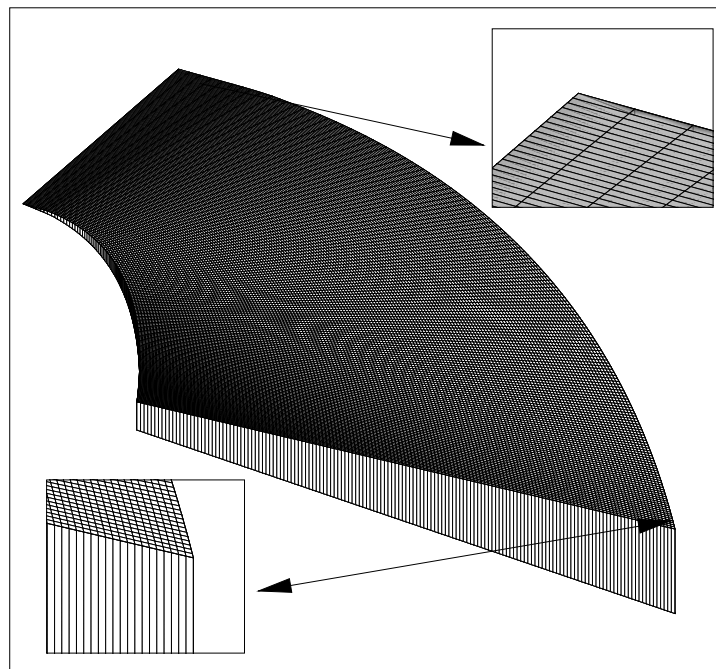


Figure 14: Axisymmetric blunt body mesh configuration

The axisymmetric mesh configuration (Fig.(14)), is constructed assuming symmetry about the center line and using side patches of wedge type (OpenCFD-Ltd, 2010). It has 24500 hexahedral cells. Since the van Leer limiter provide good behavior about shock capturing and oscillations free pressure fields in the two dimensional blunt body case, it was also used here.

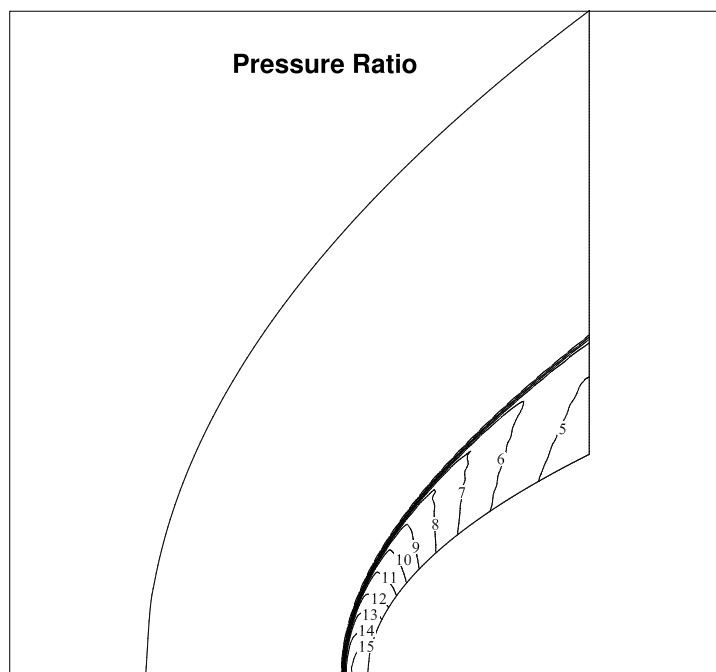


Figure 15: Pressure contour lines

From Fig.(16), it is seen that pressure coefficients predicted by *rhoCentralFoam* and Newtonian theory are in fair agreement. Notice that in this calculation the impact pressure error is 1.6%.

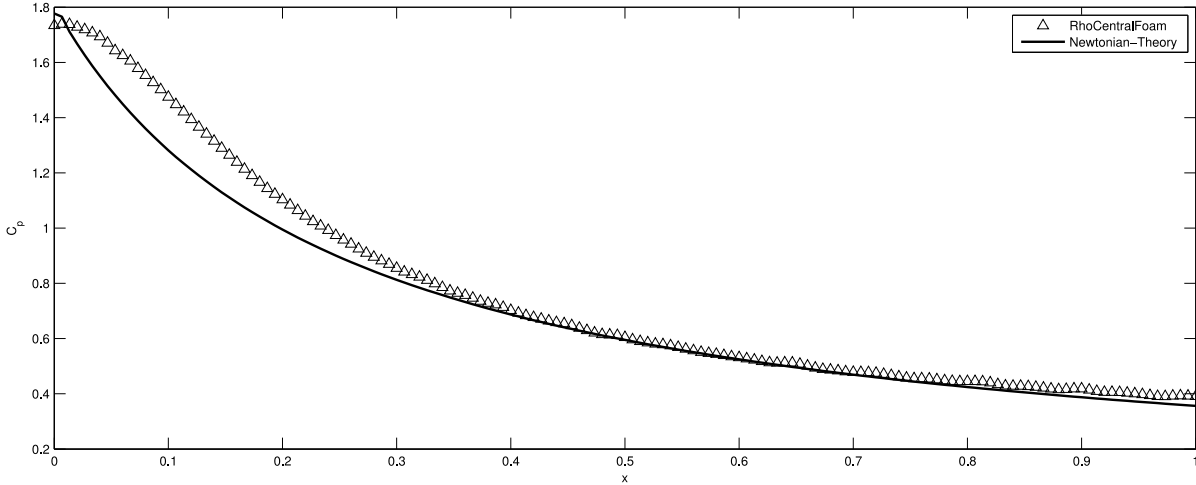


Figure 16: Pressure coefficient

5 CONCLUSIONS

As a comprehensive conclusion of this study, it can be stated that *rhoCentralFoam* performs better than *sonicFoam* in handling supersonic flow simulations. This conclusion, reached after the consideration of several case studies, is mainly supported by the use in *rhoCentralFoam* of the central-upwind schemes proposed by Kurganov and others, being competitive with the best developed schemes involving Riemann solvers and, in addition, is simpler and well suited for the construction of flux interpolations which must comply with the premise that in compressible flows, properties are not only transported by the flow velocity but also by the propagation of waves. On the other hand, *sonicFoam* developed as pressure based solver uses the PISO method, originally designed for incompressible flow and later patched by Issa and others with extra steps to extend its application to compressible flows. Thus, to obtain correct results, it is needed to preserve the coupling pressure-density through the equation of state and for this reason, the energy equation must be added to PISO loops. However, still remains as PISO main feature the decoupling of pressure from velocity, but in supersonic flows where interactions between local quantities are totally dominant, the PISO approach may not be the best choice, if there is any. A fundamental limitation of density based solvers exist close to the incompressible limit ($M < 0.3$). But in these low speed cases, with rapidly changing temperature distributions, strong density variations (e. g., chemically reacting flows) and hence compressibility effects are manifested, the extended PISO technique has proved to be useful.

From the numerical simulations it has been found that *sonicFoam* may need as much as three times more cells than *rhoCentralFoam* to obtain results of comparable quality. When the number of cells is the same, the computer time of *sonicFoam* is already greater and the results may not properly describe the physical solution. Regarding *rhoCentralFoam*, it can be stated that the van Leer limiter compared to Minmod and van Albada limiters, provides the best performance balance accounting for oscillations free fields, shock capture, required number of cells and computational cost.

REFERENCES

- Anderson J. *Modern Compressible Flow: With Historical Perspective*. McGraw-Hill Series in Aeronautical and Aerospace Engineering. McGraw-Hill, 2004. ISBN 9780071241366.
- Anderson J. *Hypersonic and High-Temperature Gas Dynamics*. AIAA Education Series. American Institute of Aeronautics and Astronautics, 2006.
- Billig F. Shock-wave shapes around spherical-and cylindrical-nosed bodies. *Journal of Spacecraft and Rockets*, 4:822–823, 1967.
- Brooks G. and Powers J. Standardized pseudospectral formulation of the inviscid supersonic blunt body problem. *Journal of Computational Physics*, 197(1):58–85, 2004.
- Chung T.J. *Computational Fluid Dynamics*. Cambridge University Press, 2 edition, 2010.
- Favre A. Statistical equations of turbulent gases. *Problems of hidrodynamics and continuum mechanics*, pages 231–266, 1969.
- Greenshields C., Weller H., Gasparini L., and Reese J. Implementation of semi-discrete, non-staggered central schemes in a colocated, polyhedral, finite volume framework, for high-speed viscous flows. *International journal for numerical methods in fluids*, 63(1):1–21, 2010.
- Issa R. Solution of the implicitly discretised fluid flow equations by operator-splitting. *Journal of computational physics*, 62(1):40–65, 1985.
- Kurganov A., Noelle S., and Petrova G. Semidiscrete central-upwind schemes for hyperbolic conservation laws and hamilton – jacobi equations. *J. Comput. Phys*, 160:720–742, 2000.
- Kurganov A. and Tadmor E. New high-resolution central schemes for nonlinear conservation laws and convection – diffusion equations. *Journal of Computational Physics*, 160(1):241 – 282, 2000.
- OpenCFD-Ltd. openfoam: user guide, 2010.
- Poinsot T. and Lelef S. Boundary conditions for direct simulations of compressible viscous flows. *Journal of computational physics*, 101(1):104–129, 1992.
- Romanelli G., Serioli E., and Mantegazza P. A new accurate compressible inviscid solver for aerodynamic applications. 3rd OpenFOAM Workshop by Dipartimento di Energetica, Politecnico di Milano, Milan Italy, 2010.
- Weller H., Tabor G., Jasak H., and Fureby C. A tensorial approach to computational continuum mechanics using object orientated techniques. *Comp. in Phys.*, 12(6):620–630, 1998.
- Wilcox D.C. *Turbulence modeling for CFD*. DCW Industries, California, US, 1998.